Journal of X-Ray Science and Technology 23 (2015) 473–480
DOI 10.3233/XST-150502
IOS Press

Dedicated mobile volumetric cone-beam computed tomography for human brain imaging: A phantom study

Jong-Hyun Ryu[a], Tae-Hoon Kim[a], Chang-Won Jeong[a], Hong-Young Jun[a], Dong-Woon Heo[a], Jinseok Lee[a], Kyong-Woo Kim[c] and Kwon-Ha Yoon[a,b,*]
[a]*Imaging Science-based Lung and Bone Disease Research Center, Wonkwang University, Iksan, Jeonbuk, Korea*
[b]*Department of Radiology, Wonkwang University School of Medicine, Iksan, Jeonbuk, Korea*
[c]*Nanofocusray, Deokjin-gu, Jeonju, Jeonbuk, Korea*

Received 11 November 2014
Revised 28 April 2015
Accepted 23 May 2015

Abstract.
BACKGROUND: Mobile computed tomography (CT) with a cone-beam source is increasingly used in the clinical field. Mobile cone-beam CT (CBCT) has great merits; however, its clinical utility for brain imaging has been limited due to problems including scan time and image quality.
OBJECTIVE: The aim of this study was to develop a dedicated mobile volumetric CBCT for obtaining brain images, and to optimize the imaging protocol using a brain phantom.
METHODS: The mobile volumetric CBCT system was evaluated with regards to scan time and image quality, measured as signal-to-noise-ratio (SNR), contrast-to-noise-ratio (CNR), spatial resolution (10% MTF), and effective dose. Brain images were obtained using a CT phantom.
RESULTS: The CT scan took 5.14 s at 360 projection views. SNR and CNR were 5.67 and 14.5 at 120 kV/10 mA. SNR and CNR values showed slight improvement as the x-ray voltage and current increased ($p < 0.001$). Effective dose and 10% MTF were 0.92 mSv and 360 μm at 120 kV/10 mA. Various intracranial structures were clearly visible in the brain phantom images.
CONCLUSIONS: Using this CBCT under optimal imaging acquisition conditions, it is possible to obtain human brain images with low radiation dose, reproducible image quality, and fast scan time.

Keywords: Cone-beam computed tomography, volumetric computed tomography, dedicated mobile CT, brain imaging

1. Background

Mobile computed tomography (CT) for brain imaging is clinically useful and cost-effective when employed in the intensive care unit (ICU), operating room, or emergency department, because it elim-

*Corresponding author: Kwon-Ha Yoon, Department of Radiology, Wonkwang University School of Medicine and Hospital, 344-2 Sinyong-dong, Iksan, Jeonbuk 570-749, Korea. Tel.: +82 63 859 1921; Fax: +82 63 851 4749; E-mail: khy1646@wonkwang.ac.kr.

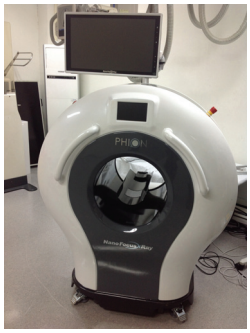

Fig. 1. Photograph of the mobile cone-beam computed tomography (CT) scanner for brain imaging. The CT system is linked to the hospital PACS system. (Colours are visible in the online version of the article; http://dx.doi.org/10.3233/XST-150502)

inates the risk of transportation-related adverse events and saves time [2,26]. Previous studies have reported the incidence of adverse events during patient transport to be as high as 71%. This risk may reach 15% even with a well-trained transport team; therefore, it is important to limit patient transport [3]. Clinical applications of mobile CT brain imaging include intraoperative evaluations for central nervous system surgery, cerebral edema, suspected hydrocephalus, suspected bleeds, cerebral infarct localization, and skull base applications, among others [17,26].

Mobile CT techniques have been designed using 2 different approaches. One is volumetric cone-beam CT (CBCT), which is already used in micro- and dental-CT applications. The other is conventional fan-beam multi-detector CT (MDCT). CBCT offers smaller, less expensive, and more maneuverable equipment. It requires a lower effective radiation dose and a shorter scan time compared to MDCT. The limitations of CBCT include a small field-of-view (FOV), and artifacts such as rings, streaks, and motion [29]. The FOV of CBCT is limited by the flat-panel detector size, but the half-scan cone-beam technique (offset scan method) can be used to increase the FOV [24]. Ring artifacts are troublesome in flat-panel detector-based volumetric CBCT because they can degrade image quality, but these artifacts can be removed using image processing on sonograms [12,23]. Mobile MDCT has typically been used for brain scanning, and CBCT systems have only recently been designed for imaging of the sinus, skull, temporal bone, and extremities [4,10,27]. Until now, there has been no dedicated mobile volumetric CBCT for human brain imaging [8].

Recently, we developed a novel dedicated mobile volumetric CBCT for brain imaging using a complementary metal oxide semiconductor (CMOS) detector. Due to the substantial increase in CT usage, optimization of proper CT imaging protocols is critical [23]. We measured the performance of this system including scan time, spatial resolution, contrast-to-noise ratio (CNR), signal-to-noise ratio (SNR), and effective dose, according to various x-ray conditions and number of projection views (PV*no*). The use of mobile dedicated CBCT with an optimized brain imaging protocol may be helpful for critically ill patients, because this system delivers a low radiation dose. In this paper, we report the performance of the CBCT for dedicated brain imaging using a brain phantom.

2. Materials and methods

2.1. System configuration

A dedicated mobile volumetric CBCT (Phion^{TM}, NanoFocusRay Ltd, Jeonju, Korea) for brain imaging using a stationary anode cone-beam x-ray source and a flat-panel detector with a CMOS sensor (Dexela

2923, PerkinElmer, USA) was used. The CMOS sensor has 3888 × 3072 pixels with 75 μm pixel pitch and a 600 μm CsI scintillator. And it can grab 70 frames per second using 2 binned mode. We did not use anti-scatter grid. The x-ray source could generate 50–130 kV and 4–10 mA with a 500 μm focal spot size. The FOV of the mobile CBCT for brain imaging was 221 mm (XY) × 163 mm (Z), and the voxel size was 215 μm^3 in 1024 (XY) × 796 (Z). The shortest scan time of this volumetric CBCT was 5.14 s. The entire system is shown in Fig. 1. The scanner weighs approximately 275 kg, and is 1.15 m wide, 0.88 m deep, and 1.43 m tall. A Feldkamp back-projection algorithm [21] was used for image reconstruction and for generating a pre-processed sinogram. We adapted Yousuf's algorithm [23] for ring artifact reduction to the 3D sinogram obtained from the 2D projection set.

2.2. Image acquisition

For image acquisition, we specified the data acquisition and x-ray generation conditions as follows. The data acquisition conditions were defined as 360 (PV*no*.360), 480 (PV*no*.480), 720 (PV*no*.720), and 1440 (PV*no*.1440) projection views. The x-ray voltage was defined as 110 kV, 120 kV, and 130 kV, and current was defined as 8 mA, 9 mA, and 10 mA. Combinations of each condition were quantitatively analyzed according to image quality parameters and effective dose. The obtained images were pre-processed into 2D projection images in parallel, to decrease image-processing time. The brain CT images were obtained using a brain phantom (Angiographic CT head phantom ACS, Herago®, Japan).

2.3. Analysis of image quality

We analyzed image quality according to the x-ray generation condition and acquisition protocol. The criteria generally used for objective image quality assessment are the determinations of SNR, CNR, and spatial resolution [22]. SNR and CNR are the ratio of the input signal to background noise, and a description of the contrast potential in the image, respectively [5,6,16,19]. The SNR was calculated as the ratio of the bone equivalent material value (400 mgHA/cm^3) and noise. The CNR was calculated as the ratio of water-air contrast and noise. Both the SNR and CNR were mean values obtained using three image sets for each condition. The modulation transfer function (MTF) has generally been used to characterize the spatial resolution of imaging systems [6,9]. There are some basic methods for MTF calculation such as the line-spread function, the point spread function, and usage of a line pattern [3,18]. We used the line-spread method with a CT phantom (QRM-ConeBeam, QRM GmbH, Germany) to generate MTF curves.

All statistical analysis was performed with one-way anal ysis of variance (ANOVA) using the statistical package for the social sciences (SPSS version 17.0 Chicago, IL, USA). Coefficient of variance (CV) was calculated for the variability of SNR and CNR in the CT measurements. The variations in CT signals according to different x-ray conditions were analyzed by ANOVA with a Tukey post hoc adjustment, to test for significant interactions between each conditions.

2.4. Measurement of effective radiation dose

We calculated the effective dose using the method described by the International Commission on Radiological Protection (ICRP 2007) [11]. The radiation dose measurement was performed using thermoluminescent dosimeter chips (TLD-200; CaF_2: Dy, Thermo Scientific, USA). One chip was positioned at each of 27 locations within the head and neck region of an ATOM® dosimetry verification phantom

Table 1
Radiation effective dose according to the location of TLD chips at the 120 kV/10 mA condition

TLD No.	Organ	Level	Dose (mGy)	TLD No.	Organ	Level	Dose (mGy)
1	Brain, parietal	2	5.44	15	Orbit of right eye	5	8.28
2	Cranium, left parietal	3	6.91	16	Brain, mid	5	6.47
3	Cranium, frontal	3	5.87	17	Brain, mid	5	6.34
4	Cranium, right parietal	3	7.58	18	Mandible, left	7	6.36
5	Cranium, occipital	3	6.39	19	Mandible, right	7	7.36
6	Brain, left frontal	3	6.20	20	Mandible, left	8	4.22
7	Brain, right frontal	3	5.98	21	Mandible, right	8	4.27
8	Brain, left temporal	3	6.28	22	Cervical spine	8	4.51
9	Brain, right temporal	3	6.43	23	Mandible, left	9	1.08
10	Brain, left frontal	4	6.06	24	Mandible, right	9	1.22
11	Brain, right frontal	4	6.05	25	Thyroid, left	10	1.03
12	Brain, left temporal	4	6.82	26	Thyroid, right	10	1.05
13	Brain, right temporal	4	6.76	27	Cervical spine	10	0.85
14	Orbit of left eye	5	8.25				

Abbreviation: TLD, thermoluminescent dosimeter.

Table 2
The SNR, CNR, and spatial resolution according to different x-ray conditions

Voltage	Current	SNR			CNR			Spatial
(kV)	(mA)	(Mean $\pm$ SD) [CV]*	P-value†	P-value‡	(Mean $\pm$ SD) [CV]*	P-value†	P-value‡	resolution§ (μm)
110	8	4.884 $\pm$ 0.159 [3]	< 0.001	< 0.001	11.627 $\pm$ 0.231 [2]	< 0.001	< 0.001	357.1
	9	5.228 $\pm$ 0.135 [3]			12.284 $\pm$ 0.317 [3]			359.7
	10	5.331 $\pm$ 0.119 [2]			12.981 $\pm$ 0.211 [2]			387.6
120	8	5.115 $\pm$ 0.120 [2]	< 0.001		12.784 $\pm$ 0.218 [2]	< 0.001		378.8
	9	5.337 $\pm$ 0.089 [2]			13.554 $\pm$ 0.298 [2]			375.9
	10	5.677 $\pm$ 0.139 [2]			14.505 $\pm$ 0.308 [2]			359.7
130	8	5.303 $\pm$ 0.156 [3]	< 0.001		13.721 $\pm$ 0.330 [2]	< 0.001		354.6
	9	5.528 $\pm$ 0.098 [2]			14.694 $\pm$ 0.376 [3]			347.2
	10	5.834 $\pm$ 0.146 [2]			15.358 $\pm$ 0.310 [2]			378.8

Abbreviations: SD, standard deviation; CV, coefficient of variation; SNR, signal to noise ratio; CNR, contrast to noise ratio
*CV indicates the percentage of the coefficient of variation ([SD/Mean value] $\times$ 100). †Statistical analysis at each different mA value was performed with a one-way analysis of variation (ANOVA) test using a Tukey post-hoc adjustment. ‡The difference according to different kV was analyzed with a one-way ANOVA test. §Spatial resolution was calculated by 10% MTF (modulation transfer function) using the pattern of the cone-beam CT phantom.

(701-HN-D; CIRS, USA). Each TLD chip ID, organ, and phantom level is displayed in Table 1. Radiation experiments were repeated three times and the average was used to obtain the radiation value. Ten additional chips were kept outside the scanning room to allow for a later determination and subtraction of the mean accumulated background radiation dose [13]. The radiation-weighted dose was multiplied by the obtained radiation value of these TLD chips and the estimated percentage of tissue irradiated. Final effective dose was calculated by the summation of the multiplied radiation weighted dose and tissue weighting factors [15,28].

3. Results

We successfully obtained a brain phantom image using the dedicated mobile CBCT with a short acquisition time. The CT scan times were 5.14 s for PV*no*.360, 6.85 s for PV*no*.480, 10.28 s for PV*no*.720, and 20.56 s for PV*no*.1440. The exposure times were 2.67, 3.43, 5.14, and 10.28 s at each PV*no*, respectively. Effective dose based on the ICRP 2007 method was 0.92 mSv at the condition of 120 kV/10 mA

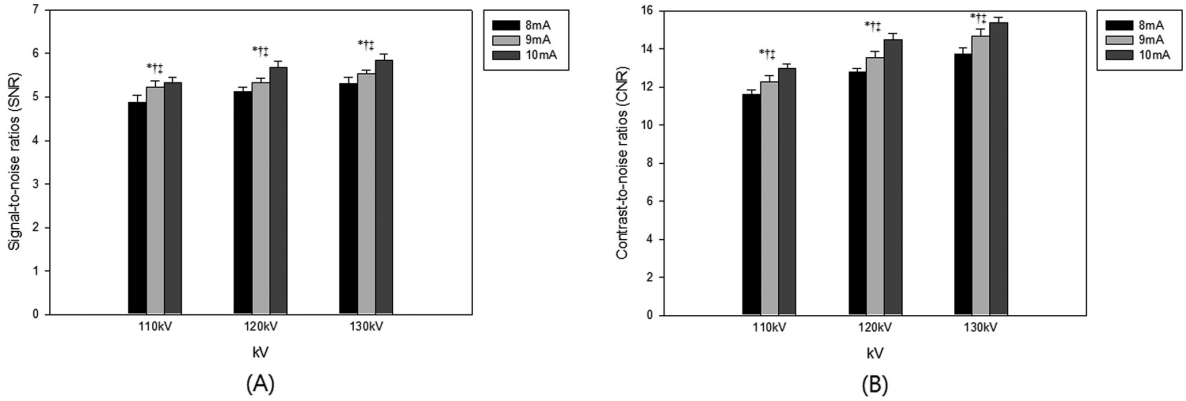

Fig. 2. Bar graph demonstrating the signal to noise ratio (SNR; A) and the contrast to noise ratio (CNR; B) for each condition. The SNR and CNR values showed a slight increase as the voltage and current of the x-ray increased ($p < 0.001$). Overall, the condition at 130 kV/10 mA showed the best values in the various conditions of x-ray currents and voltages. All of the SNR and CNR values are expressed as mean $\pm$ standard deviation (SD). *†‡indicates significant difference using the Tukey post-hoc test: * 8 mA vs 9 mA; †9 mA vs 10 mA; and ‡10 mA vs 8 mA.

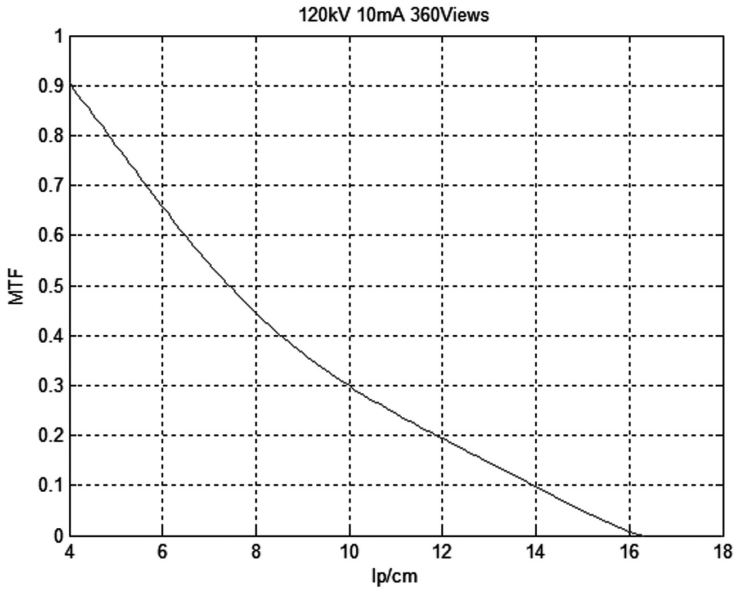

Fig. 3. MTF Curve of the optimal protocol (120 kV/10 mA and PV*no*.360).10% MTF was 13.9 lp/(359.7 μm).

and 1.75 mSv at the condition of 130 kV/10 mA (Table 1). The SNR, CNR, and spatial resolution according to each x-ray condition are summarized in Table 2 and Fig. 2. The SNR and CNR values showed a slight improvement as the voltage and current of the x-ray increased ($p < 0.001$). Overall, the 130 kV/10 mA condition showed the best values out of all the various conditions of x-ray currents and voltages. The spatial resolution at a condition of 120 kV/10 mA was better than that at 130 kV/10 mA. Therefore, the condition of 120 kV/10 mA and PV*no*.360 was optimal to obtain human brain imaging based on the SNR, CNR, MTF, scan time and effective dose. Figure 3 shows MTF curve of the optimal protocol. And Fig. 4 shows the CT images of a brain phantom under the preferred image acquisition conditions. Various intracranial structures are clearly distinguishable.

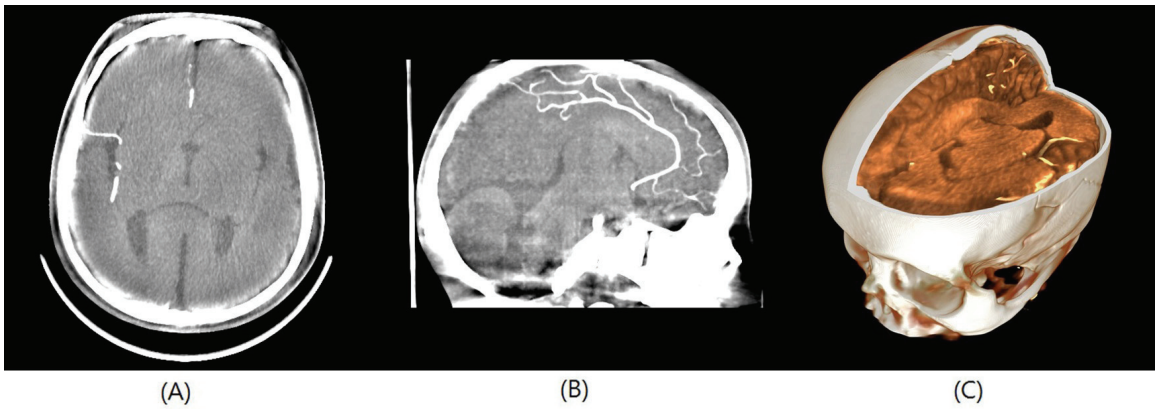

Fig. 4. Computed tomography (CT) images of the axial (A) and sagittal (B) planes of the brain phantom as obtained with the mobile volumetric cone-beam computed tomography (CBCT) system. The intracranial vessels and various brain structures are clearly seen. The brain structure is also shown on a multiplanar rendering image (C). (Colours are visible in the online version of the article; http://dx.doi.org/10.3233/XST-150502)

4. Discussion

In this study, we successfully developed a novel volumetric CBCT with a CMOS detector for dedicated brain imaging. Mobile brain CT has been used for intraoperative evaluation of the extent of tumor resection, early assessment of re-bleeding after craniotomy, and skull base applications. Brain scanning using mobile CT is also used for the evaluation of cerebral edema, suspected hydrocephalus, suspected bleeds, and cerebral infarct localization. Although it is well known that CBCT has several disadvantages including a small FOV and artifacts, mobile CBCT has the advantages of lower cost, smaller size, lighter weight, and lower radiation dose as contrasted with mobile MDCT. Taking all the information, we initiated to develop a novel dedicated mobile volumetric CBCT for brain imaging.

Present study adapted a flat-panel CMOS detector with a CsI scintillator in this CBCT system. A flat panel CMOS x-ray detector has many features necessary for brain imaging, including a high frame-rate, low read noise, high reliability, high detective quantum efficiency (DQE), and high spatial resolution. Because the CMOS detector can obtain projections at a high frame rate, the radiation dose for the patient can be minimized. Our CBCT could acquire 360 projection images of 360 degrees within 5.14 s using a combination of the CMOS detector and a camera link interface. The high speed of acquisition is sufficient to obtain a brain perfusion image. Ring artifacts are a significant problem in flat-panel detector-based volumetric CBCT because they can degrade image quality. Unlike ring artifacts in other types of CBCT, such as image intensifier-based CT, ring artifacts in flat-panel detector-based CBCT are not removable [12,23]. To reduce ring artifacts, this system used an algorithm either before or after CT reconstruction. This system used "monoblock" technology, where the x-ray tube and the high-voltage generator are incorporated into a single casing. This reduces the size and cost of the x-ray tube. The closer the x-ray tube is to the patient, the less power is needed for diagnostic image quality.

Recently angiographic CBCT have been used in clinical interventional radiology suite [27]. A study had shown that image quality of angiography flat-panel CT with low dose protocol is not enough to diagnosis of brain parenchyma for signs of ischemia [27]. On the contrary, the image quality with high dose protocol is possible to diagnose the patient. Therefore, brain protocol optimization is essential for medical imaging equipment, particularly concerning the effective radiation dose and image quality. To optimize this brain imaging protocol, we defined several protocol conditions for the x-ray in this study.

In terms of image quality, a study reported that CNR of other volumetric CTs are 8.2–18.8 and 10% MTF are 0.1–0.8/mm^{-1} [7]. With our system, SNR and CNR increased as the voltage and current of the x-ray and number of projection views increased. That is, SNR, CNR and 10% MTF at each condition (minimum to maximum) were 4.9–5.8, 11.6–15.4 and 347–387 μm, respectively. With regard to effective dose, a study reported that effective dose of CBCT using flat-panel detector with low-dose protocol was approximately 1.0-mSv and effective dose of conventional CT was 17.8 mSv [27]. Effective doses of our system were 0.92 mSv at the condition of 120 kV/10 mA and 1.75 mSv at the condition of 130 kV/10 mA. Although 10% MTF of 130 kV/9 mA condition were better than 120 kV/10 mA condition, effective dose of 130 kV/9 mA protocol was much higher than that of 120 kV/10 mA protocol. There were some opposite results. In this regards, we considered that the effective dose to the patients is more important than that of spatial resolution in diagnostic imaging.

Acquisition time of our system was 5.14 seconds at 360 projection views. On the contrary, other commercialized volumetric CT scanner of dedicated extremity CBCT (Planmed Verity, Finland) is 18 seconds. Maxillofacial CBCT such as i-CAT (Imaging Sciences International, USA), CB Mercuray (Hitachi, Japan), AZ3000CT (Asahi, Japan), Promax (Planmeca, USA), Implagraphy (Vatrech, Korea), and 3D EXAM (Kavo, Germany) are 8.9, 10, 17, 18, 19, and 26.9 seconds, respectively [1,14,25].

When we used the low x-ray voltage less than 100 kV, the beam hardening artifacts were increased markedly on CT images. It was not enough to obtain the images of brain parenchyma via skull bone. Therefore, we did not study using less than 100 kV. By taking the SNR, CNR, MTF, scan time, and effective dose into account, we could choose the optimal protocol: 120 kV, 10 mA, 360 projection views and scan time of 5.14 seconds. Therefore, the proposed image quality data and effective dose were acquired at the same setting condition. The increase of x-ray and projection views caused increase effective dose to the patients. We have chosen that protocol of higher radiation dose is not appropriate protocol for brain imaging on this mobile CT. The calculated effective dose was 0.92 mSv, and the spatial resolution with 10% MTF was 360 μm under these conditions. And our system was able to obtain high-resolution images of a brain phantom using our chosen protocol. All studies using this scanner were deemed clinically acceptable and were of appropriate diagnostic quality.

5. Conclusion

We have successfully developed a volumetric CBCT for dedicated brain imaging using a CMOS detector. We obtained high-quality brain phantom images, enabling the interpreter to distinguish major brain structures. The use of mobile dedicated CBCT with an optimized brain imaging protocol may be helpful for critically ill patients, as it delivers only a low radiation dose.

Acknowledgments

This study was supported by a grant of the Korean Health Technology R&D Project, Ministry of Health and Welfare, Republic of Korea (HI12C0110).

References

[1] A. Suomalainen, T. Kiljunen, Y. Kaser, J. Peltola and M. Kortesniemi, Dosimetry and image quality of four dental cone beam computed tomography scanners compared with multislice computed tomography scanners, *Dentomaxillofac Radiol* **38** (2009), 367–378.

[2] A.P. Carlson and H. Yonas, Portable head computed tomography scanner-technology and applications: Experience with 3421 scans, *J NeuroImaging* **22** (2012), 408–415.
[3] A.S. Chawla, H. Roehrig, J.J. Rodriguez and J. Fan, Determining the MTF of medical imaging displays using edge techniques, *J Digit Imaging* **18** (2005), 296–310.
[4] B.C. Campbell, S. Christensen, C.R. Levi, P.M. Desmond, G.A. Donnan, S.M. Davis and M.W. Parsons, Cerebral blood flow is the optimal CT perfusion parameter for assessing infarct core, *Stroke* **42** (2011), 3435–3440.
[5] C.M. Heyer, P.S. Mohr, S.P. Lemburg, S.A. Peters and V. Nicolas, Image quality and radiation exposure at pulmonary CT angiography with 100-or 120-kVp protocol: prospective randomized study, *Radiology* **245** (2007), 577–583.
[6] D.G. Brown and R.F. Wagner, Physics and statistics of medical imaging, *J Digit Imaging* **2** (1989), 194–211.
[7] G. d'Assignies, A. Couvelard, S. Bahrami, M.P. Vullierme, P. Hammel, O. Hentic, A. Sauvanet, P. Bedossa, P. Ruszniewski and V. Vilgrain, Pancreatic endocrine tumors: Tumor blood flow assessed with perfusion CT reflects angiogenesis and correlates with prognostic factors, *Radiology* **250** (2009), 407–416.
[8] D.K. Jeong, S.-C. Lee, K.H. Huh, W.-J. Yi, M.S. Heo, S.S. Lee and S.C. Choi. Comparison of effective dose for imaging of mandible between multi-detector CT and cone-beam CT, *Imaging Science in Dentistry* **42** (2012), 65–70.
[9] H. Fujita, D.Y. Tsai, T. Itoh, K. Doi, J. Morishita, K. Ueda and A. Ohtsuka, A simple method for determining the modulation transfer function in digital radiography, *IEEE Trans Med Imaging* **11** (1992), 34–39.
[10] H.C. Roberts, T.P. Roberts, T.Y. Lee and W.P. Dillon, Dynamic, contrast-enhanced CT of human brain tumors: quantitative assessment of blood volume, blood flow, and microvascular permeability: Report of two cases, *AJNR Am J Neuroradiol* **23** (2002), 828–832.
[11] International Commission on Radiological Protection (ICRP), The 2007 recommendations of the International Commission on Radiological Protection. ICRP publication 103, *Ann ICRP* **37** (2007), 1–332.
[12] J. Sijbers and A. Postnov, Reduction of ring artefacts in high resolution micro-CT reconstructions, *Phys Med Biol* **49** (2004), N247–N253.
[13] J.A. Roberts, N.A. Drage, J. Davies and D.W. Thomas, Effective dose from cone beam CT examinations in dentistry, *Br J Radiol* **82** (2009), 35–40.
[14] J.B. Ludlow and M. Ivanovic, Comparative dosimetry of dental CBCT devices and 64-slice CT for oral and maxillofacial radiology, *Oral Surgery Oral Medicine Oral Pathology Oral Radiology and Endodontology* **106** (2008), 106–114.
[15] J.B. Ludlow, L.E. Davies-Ludlow, S.L. Brooks and W.B. Howerton, Dosimetry of 3 CBCT devices for oral and maxillofacial radiology: CB Mercuray, NewTom 3G and i-CAT, *Dentomaxillofac Radiol* **35** (2006), 219–226.
[16] J.T. Bushberg, J.A. Seibert, E.M. Leidholdt, Jr. and J.M. Boone, The essential physics of medical imaging, 2nd edition, Lippincott Williams & Wilkins, Philadelphia, 2002, pp. 262, 278, 367–369.
[17] K. Peace, E.M. Wilensky, S. Frangos, E. MacMurtrie, E. Shields, M. Hujcs, J. Levine, A. Kofke, W. Yang and P.D. Le Roux, The use of a portable head CT scanner in the intensive care unit, *J Neurosci Nurs* **42** (2010), 109–116.
[18] K. Rossman, Point spread-function, line spread-function, and modulation transfer function. Tools for the study of imaging systems, *Radiology* **93** (1969), 257–272.
[19] K. Seet, A. Barghi, S. Yartsev and J. Van Dyk, Optimal slice thickness for cone-beam CT with on-board imager, *Biomed Imaging Interv J* **6** (2010), 1–4.
[20] K.L. Dobeli, S.J. Lewis, S.R. Meikle, D.L. Thiele and P.C. Brennan, Optimization of computed tomography protocols: Limitations of a methodology employing a phantom with location-known opacities, *J Digit Imaging* **26** (2013), 1001–1007.
[21] L.A. Feldkamp, L.C. Davis and J.W. Kress, Practical cone-beam algorithm, *J Opt Soc Am* **1** (1984), 612–619.
[22] L.W. Goldman, Principles of CT: Radiation dose and image quality, *J Nucl Med Technol* **35** (2007), 213–225.
[23] M.A. Yousuf and M. Asaduzzaman, An efficient ring artifact reduction method based on projection data for micro-CT images, *J Sci Res* **2** (2010), 37–45.
[24] P.S. Cho, A.D. Rudd and R.H. Johnson, Cone-beam CT from width-truncated projections, *Comput Med Imaging Graph* **20** (1996), 49–57.
[25] S.K. Koskinen, V.V. Haapamäki, J. Salo, N.C. Lindfors, M. Kortesniemi, L. Seppälä and K.T. Mattila, CT arthrography of the wrist using a novel, mobile, dedicated extremity cone-beam CT (CBCT), *Skeletal Radiology* **42** (2013), 649–657.
[26] T. Masaryk, R. Kolonick, T. Painter and D.B. Weinreb, The economic and clinical benefits of portable head/neck CT imaging in the intensive care unit, *Radiol Manage* **30** (2008), 50–54.
[27] T. Struffert, Y. Deuerling-Zheng, S. Kloska, T. Engelhorn, C.M. Strother, W.A. Kalender, M. Köhrmann, S. Schwab and A. Doerfler, Flat detector CT in the evaluation of brain parenchyma, intracranial vasculature, and cerebral blood volume: A pilot study in patients with acute symptoms of cerebral ischemia, *AJNR Am J Neuroradiol* **31** (2010), 1462–1469.
[28] T.A. Jaffe, J.K. Hoang, T.T. Yoshizumi, G. Toncheva, C. Lowry and C. Ravin, Radiation dose for routine clinical adult brain CT: Variability on different scanners at one institution, *AJR Am J Roentgenol* **195** (2010), 433–438.
[29] Z. Rumboldt, W. Huda and J.W. All, Review of portable CT with assessment of a dedicated head CT scanner, *AJNR Am J Neuroradiol* **30** (2009), 1630–1636.